Journal of Hydrology 408 (2011) 127–139

Contents lists available at ScienceDirect

Journal of Hydrology

journal homepage: www.elsevier.com/locate/jhydrol

A new Iterative Alternating Direction Implicit (IADI) algorithm for multi-dimensional saturated–unsaturated flow

Hyunuk An [a,*], Yutaka Ichikawa [b], Yasuto Tachikawa [c], Michiharu Shiiba [c]

[a] Graduate School of Engineering, Kyoto University, Nishikyoku, Kyoto 615-8540, Japan
[b] Interdisciplinary Graduate School of Medicine and Engineering, University of Yamanashi, Kofu, Yamanashi 400-8511, Japan
[c] Faculty School of Engineering, Kyoto University, Nishikyoku, Kyoto 615-8540, Japan

ARTICLE INFO

Article history:
Received 20 July 2010
Received in revised form 1 June 2011
Accepted 21 July 2011
Available online 29 July 2011

This manuscript was handled by Philippe Baveye, Editor-in-Chief, with the assistance of Nunzio Romano, Associate Editor

Keywords:
Richards equation
Saturated–unsaturated flow
ADI scheme
Finite difference model

SUMMARY

Numerical simulation of saturated–unsaturated subsurface flows is widely used in many branches of science and engineering, and rapid developments in computer technology have enabled not only one-dimensional but also multi-dimensional simulations on a personal computer. However, a multi-dimensional subsurface flow simulation still incurs heavy load on computational resources, particularly for simulations in wide regions with long periods. An Iterative Alternating Direction Implicit (IADI) scheme has certain advantages in terms of computational cost and algorithmic simplicity. However, it is barely used at present because it occasionally incurs numerical instabilities and convergence difficulties. Another reason is that three-dimensional simulations cannot be performed by the original IADI scheme. This study has proposed an advanced IADI algorithm for solving the saturated–unsaturated flow equation; this advanced scheme is more numerically stable than the original IADI scheme and can be used for three-dimensional simulations. The performance of the proposed scheme was assessed through test simulations. In all the simulations, the new method was shown to be faster than the fully implicit scheme linearized by the modified Picard iteration method while still yielding very similar results.

1. Introduction

Numerical simulation of a saturated–unsaturated subsurface flows is widely used in many branches of science and engineering, including agricultural engineering, ground water engineering, chemical contaminants tracing, and rainfall–runoff modeling. A variety of numerical models have been proposed on the basis of the finite difference, finite element, and finite volume methods to simulate a saturated–unsaturated flow (e.g. Celia et al., 1990; Clement et al., 1994; Forsyth et al., 1995; Jones and Woodward, 2001; Manzini and Ferraris, 2004; Simunek et al., 1999; Tocci et al., 1997). In particular, methods using finite difference algorithms have demonstrated advantages in terms of the ease of coding and understanding owing to their simplicity compared with the other two methods. Rapid developments in computer technology have made it possible to carry out not only one-dimensional (Dane and Mathis, 1981; Haverkamp and Vauclin, 1981) but also multi-dimensional simulations (Clement et al., 1994; Dogan and Motz, 2005; Simunek et al., 1999; Weeks et al., 2004) using a personal computer. However, a multi-dimensional subsurface flow simulation still requires considerable computer resources, particularly for simulations in wide regions with a relatively fine grid resolution.

The alternating direction implicit (ADI) approach and Iterative ADI (IADI) were very popular in the 1970s for avoiding the solution of large, sparse linear systems arising from the implicit discretization of parabolic partial differential equations in 2D and 3D. The IADI scheme is an iterative adaption of the ADI method, which discretizes the equation into a simultaneous system of difference equations that are solved iteratively. Since then, the method has been rarely used in favor of the preconditioned Krylov subspace iteration and even sparse direct solvers. However, the IADI approach has advantages over Krylov solvers in terms of simplicity and cost (on a per iteration basis) because only tridiagonal linear systems are involved in the procedure of the calculation. Optimal Krylov subspace solvers need preconditioners based on multigrid or domain decomposition, which introduce considerably more programming complexity than the IADI method. Furthermore, the computational cost for tridiagonal linear systems is comparatively cheap and proportional to the problem dimension. This implies that the computational cost of the IADI method is expected to be scalable, while the computational cost of the preconditioned Krylov subspace solvers typically increases faster than the problem dimension does. Therefore, if the IADI algorithm overcomes shortcomings such as the instability and convergence difficulty, which will be discussed in the next paragraph, it could be an attractive

* Corresponding author. Tel.: +81 75 383 3365.
E-mail address: an@hywr.kuciv.kyoto-u.ac.jp (H. An).

0022-1694/$ - see front matter © 2011 Elsevier B.V. All rights reserved.
doi:10.1016/j.jhydrol.2011.07.030

alternative for simulating a saturated–unsaturated flow in porous media. The objective of this study is to propose an improved IADI algorithm for a multi-dimensional saturated–unsaturated flow.

The study by Rubin (1968) was probably the earliest to simulate a two-dimensional transient groundwater flow using the IADI method. Following this study, the IADI method has been used in several studies (e.g. Cooley, 1971; Parissopoulos and Wheater, 1988; Perrens and Watson, 1977; Weeks et al., 2004) to simulate a two-dimensional saturated–unsaturated flow in porous media. All these models solved the pressure-head-based form of the Richards equation (Richards, 1931). However, Celia et al. (1990) stated that numerical methods using the pressure-head-based form of the Richards equation result in a poor mass balance in the unsaturated zone because of the highly non-linear constitutive relationship between the pressure head and the moisture content. These authors showed that solutions based on a mixed form of the Richards equation are more accurate than those based on the pressure-head-based form and satisfy the mass balance. Moreover, Clement et al. (1994) claims that the IADI scheme is not robust because it incurs numerical instabilities and convergence difficulties in solving two-dimensional non-linear equations. This is one of the reasons for rarely using the IADI technique at present. The other reasons might be that the IADI scheme cannot be used for solving three-dimensional problems and that the finite difference-based scheme is limited for real multi-dimensional applications involving complex geometries. To solve the latter problem, we can consider the use of a coordinate transformation method (e.g. Jie et al., 2004; Kinouchi et al., 1991; Koo and Leap, 1998a,b; Ruhaak et al., 2008) or an adaptively refined grid approach (Li et al., 2000) in combination with the IADI scheme.

In this study, in order to overcome the numerical instabilities and applicability of the three-dimensional simulations of the original IADI method of Rubin (1968), we derived a new equation from the ADI method of Douglas and Rachford (1956). The newly derived equation can be applied to two- and three-dimensional problems and shows improved stability. To evaluate the proposed method, five test simulations were conducted, and the results were compared with those of the original IADI scheme and the fully implicit scheme linearized by the modified Picard iteration method.

2. Theory

The mixed form of the Richards equation is generally considered to have advantages in terms of the mass balance and the convergence behavior, which is written as

$$\frac{\partial\theta}{\partial t}=\nabla\cdot K(\psi)\nabla\psi+\frac{\partial K(\psi)}{\partial z}, \tag{1}$$

where ψ is the pressure head, θ is the volumetric moisture content, K is the hydraulic conductivity, t is the time, and z denotes the vertical dimension, assumed to be positive upwards. Further, it is assumed that appropriate constitutive relationships between θ and ψ and between ψ and K are available. The source/sink term has been ignored for the sake of simplicity. Because Eq. (1) includes both θ and ψ, it is called the mixed form.

2.1. Picard iterative linearization

The backward Euler scheme is one of the most widely used time approximation for the Richards equation and used in this study. Since the system of the equation is non-linear because of the non-linear dependency of θ on ψ, iterative calculation and linearization are needed. Although several iterative schemes have been proposed (e.g. Bergamaschi and Putti, 1999; Fassino and Manzini, 1998; Kavetski et al., 2002; Paniconi and Putti, 1994), from a practical viewpoint, the Picard method is used in this study because it is simple and exhibits a good performance in many problems (Lehmann and Ackerer, 1998; Paniconi and Putti, 1994). The backward Euler approximation and Picard linearization of the two-dimensional Eq. (1) is written as

$$\frac{\theta^{n+1,m+1}-\theta^{n}}{\Delta t}=\frac{\partial}{\partial x}\left\{K^{n+1,m}\frac{\partial\psi}{\partial x}\Big|^{n+1,m+1}\right\}+\frac{\partial}{\partial z}\left\{K^{n+1,m}\frac{\partial\psi}{\partial z}\Big|^{n+1,m+1}\right\}+\frac{\partial K}{\partial z}\Big|^{n+1,m}, \tag{2}$$

where the superscripts n and m denote the time level and the iteration level, and x denotes the horizontal dimension.

The moisture content at the new time step and a new iteration level ($\theta^{n+1,m+1}$) is replaced with the Taylor series expansion with respect to ψ, about the expansion point $\psi^{n+1,m}$ as follows:

$$\theta^{n+1,m+1}=\theta^{n+1,m}+\frac{d\theta}{d\psi}\Big|^{n+1,m}(\psi^{n+1,m+1}-\psi^{n+1,m})+O(\delta^2). \tag{3}$$

Neglecting the higher-order terms in Eq. (3) and substituting this equation into Eq. (2) gives

$$C^{n+1,m}\frac{\psi^{n+1,m+1}-\psi^{n+1,m}}{\Delta t}+\frac{\theta^{n+1,m}-\theta^{n}}{\Delta t}=\frac{\partial}{\partial x}\left\{K^{n+1,m}\frac{\partial\psi}{\partial x}\Big|^{n+1,m+1}\right\}+\frac{\partial}{\partial z}\left\{K^{n+1,m}\frac{\partial\psi}{\partial z}\Big|^{n+1,m+1}\right\}+\frac{\partial K}{\partial z}\Big|^{n+1,m}, \tag{4}$$

where $C(=d\theta/d\psi)$ is the specific moisture capacity function. A finite difference approximation of Eq. (4) can be written as

$$C_{i,j}^{n+1,m}\frac{\psi_{i,j}^{n+1,m+1}-\psi_{i,j}^{n+1,m}}{\Delta t}+\frac{\theta_{i,j}^{n+1,m}-\theta_{i,j}^{n}}{\Delta t}=\Delta_x(K^{n+1,m}\Delta_x\psi^{n+1,m+1})+\Delta_z(K^{n+1,m}\Delta_z\psi^{n+1,m+1})+\Delta_z(K^{n+1,m}), \tag{5}$$

where

$$\Delta_x(K^{n+1,m}\Delta_x\psi^{n+1,m+1})=\frac{1}{\Delta x^2}K_{i+1/2,j}^{n+1,m}\left(\psi_{i+1,j}^{n+1,m+1}-\psi_{i,j}^{n+1,m+1}\right)-\frac{1}{\Delta x^2}K_{i-1/2,j}^{n+1,m}\left(\psi_{i,j}^{n+1,m+1}-\psi_{i-1,j}^{n+1,m+1}\right),$$

$$\Delta_z(K^{n+1,m}\Delta_z\psi^{n+1,m+1})=\frac{1}{\Delta z^2}K_{i,j+1/2}^{n+1,m}\left(\psi_{i,j+1}^{n+1,m+1}-\psi_{i,j}^{n+1,m+1}\right)-\frac{1}{\Delta z^2}K_{i,j-1/2}^{n+1,m}\left(\psi_{i,j}^{n+1,m+1}-\psi_{i,j-1}^{n+1,m+1}\right),$$

$$\Delta_z(K^{n+1,m})=\frac{K_{i,j+1/2}^{n+1,m}-K_{i,j-1/2}^{n+1,m}}{\Delta z}, \tag{6}$$

and subscripts i and j denote the spatial coordinates in the x and z axes, respectively. Eq. (5) represents the same method proposed by Clement et al. (1994), except that this equation ignores the specific storage term. These linearized simultaneous equations are solved using matrix solvers such as the LU decomposition or preconditioned conjugated gradient methods. In this study, LIS (a library of iterative solvers for linear systems), developed by Kotakemori et al. (2005), was used for solving the linear equations. LIS provides several preconditioners and iterative solvers for linear systems. Conducting the test simulations, we selected a pair of SSOR preconditioner and biconjugate gradient stabilized (BICGSTAB) methods, which was shown to be faster and more stable than the other pairs provided by the LIS library. The pressure head at the (n+1)th time level and the (m+1)th Picard iteration level were obtained solving

Eq. (5). The iteration process of Eq. (5) continues until the difference between the calculated values of the pressure head of the two successive iteration levels becomes less than the tolerances, until the following inequality is satisfied for all grid points:

$$|\psi^{n+1,m+1} - \psi^{n+1,m}| \leqslant \delta_\psi. \tag{7}$$

where δ_ψ is the convergence tolerance, whose value is sufficiently small enough to neglect. In this paper, $\delta_\psi = 10^{-4}$ m was used.

2.2. Original IADI scheme

If using a fine mesh, normal implicit schemes such as Eq. (5) result in a significantly large CPU cost. However, the IADI method can carry out these calculations more efficiently because large simultaneous equations do not need to be solved using the IADI algorithm.

In two-dimensional IADI procedures, each full time step is achieved by the iterative correction of two forward discretization passes. The first forward pass is based on a horizontal discretization to determine approximate values for the pressure head at the new iterative step level using the values of the current iterative level. The second forward corrective pass is based on a vertical discretization using values approximated at the first forward pass. Hence, the scheme involves performing a pair of passes to complete a full iteration.

The original IADI scheme of Rubin (1968) used the ψ-based form of the Richards equation as follows:

$$C(\psi)\frac{\partial \psi}{\partial t} = \nabla \cdot K(\psi)\nabla\psi + \frac{\partial K(\psi)}{\partial z}. \tag{8}$$

A time and spatial discretization of the two-dimensional Eq. (8) is written as

$$C_{i,j}^{n+1,2m}\frac{\psi_{i,j}^{n+1,2m+1} - \psi_{i,j}^{n}}{\Delta t} + I_m \overline{K}_{i,j}^{n}\left(\psi_{i,j}^{n+1,2m+1} - \psi_{i,j}^{n+1,2m}\right) = \Delta_x(K^{n+1,2m}\Delta_x\psi^{n+1,2m+1}) + \Delta_z(K^{n+1,2m}\Delta_z\psi^{n+1,2m}) + \Delta_z(K^{n+1,2m}), \tag{9}$$

$$C_{i,j}^{n+1,2m}\frac{\psi_{i,j}^{n+1,2m+2} - \psi_{i,j}^{n}}{\Delta t} + I_m \overline{K}_{i,j}^{n}\left(\psi_{i,j}^{n+1,2m+2} - \psi_{i,j}^{n+1,2m+1}\right) = \Delta_x(K^{n+1,2m}\Delta_x\psi^{n+1,2m+1}) + \Delta_z(K^{n+1,2m}\Delta_z\psi^{n+1,2m+2}) + \Delta_z(K^{n+1,2m}), \tag{10}$$

where

$$\overline{K}_{i,j}^{n} = K_{i-1/2,j}^{n} + K_{i+1/2,j}^{n} + K_{i,j-1/2}^{n} + K_{i,j+1/2}^{n}, \tag{11}$$

and I_m is an iteration parameter that has been used in various forms (Parissopoulos and Wheater, 1988; Perrens and Watson, 1977). In this study, $I_m = 0.55^m$ was used according to Weeks et al. (2004). If the saturated zone appeared, $C_{i,j}^{n+1,2m}$ became zero. However, there is an additional term related to $I_m\overline{K}_{i,j}^{n}$; the matrix does not become singular unless m becomes very large, which makes I_m almost zero. The convergence criterion is as follows:

$$|\psi^{n+1,2m+2} - \psi^{n+1,2m}| \leqslant \delta_\psi. \tag{12}$$

The linearized simultaneous equations of each pass can be efficiently solved using a tridiagonal matrix solver. It is supposed that these equations are derived on the basis of the ADI method of Peaceman and Rachford (1955). However, under partially saturated conditions, this scheme often induces instability on convergence and becomes inefficient.

2.3. Advanced IADI (AIADI) scheme

Here, a new IADI equation was derived on the basis of the ADI algorithm of Douglas and Rachford (1956) in order to eliminate the previously mentioned numerical instability. The Douglas–Rachford ADI scheme is developed for linear parabolic partial differential equations. This scheme is unconditionally stable for two- and three-dimensional linear parabolic partial differential equations (Douglas and Rachford, 1956), while the Peaceman–Rachford ADI method is unconditionally stable for only two-dimensional equations (Peaceman and Rachford, 1955). Although the stability is not guaranteed for the non-linear parabolic partial differential equations, we empirically found that the proposed scheme derived from the Douglas–Rachford ADI scheme can be applied to two- and three-dimensional saturated–unsaturated problems and is more stable than the original IADI scheme in two-dimensional problems.

The newly derived IADI scheme is as follows:

$$C_{i,j}^{n+1,2m}\frac{\psi_{i,j}^{n+1,2m+1} - \psi_{i,j}^{n+1,2m}}{\Delta t} + \frac{\theta_{i,j}^{n+1,2m} - \theta_{i,j}^{n}}{\Delta t} + I_m \overline{K}_{i,j}^{n+1,2m}\left(\psi_{i,j}^{n+1,2m+1} - \psi_{i,j}^{n+1,2m}\right) = \Delta_x(K^{n+1,2m}\Delta_x\psi^{n+1,2m+1}) + \Delta_z(K^{n+1,2m}\Delta_z\psi^{n+1,2m}) + \Delta_z(K^{n+1,2m}), \tag{13}$$

$$C_{i,j}^{n+1,2m}\frac{\psi_{i,j}^{n+1,2m+2} - \psi_{i,j}^{n+1,2m+1}}{\Delta t} + I_m \overline{K}_{i,j}^{n+1,2m}\left(\psi_{i,j}^{n+1,2m+2} - \psi_{i,j}^{n+1,2m+1}\right) = \Delta_z(K^{n+1,2m}\Delta_z\psi^{n+1,2m+2}) - \Delta_z(K^{n+1,2m}\Delta_z\psi^{n+1,2m}), \tag{14}$$

where

$$\overline{K}_{i,j}^{n,2m} = K_{i-1/2,j}^{n,2m} + K_{i+1/2,j}^{n,2m} + K_{i,j-1/2}^{n,2m} + K_{i,j+1/2}^{n,2m}, \tag{15}$$

and the convergence criterion is as Eq. (12). As in the original IADI scheme, Eqs. (13) and (14) can be solved using a tridiagonal matrix solver.

Eqs. (13) and (14) can be rewritten as a one-pass equation form that gives the theoretical base of the new IADI scheme. By multiplying both sides of the equation by

$$a_m = \frac{\Delta t}{C^{n+1,2m} + \Delta t I_m \overline{K}_{i,j}^{n+1,2m}}, \tag{16}$$

we obtain the following equations:

$$(I + A_x)\psi^{n+1,2m+1} = (I - A_z)\psi^{n+1,2m} + a_m\left\{\Delta_z(K^{n+1,2m}) - \frac{\theta_{i,j}^{n+1,2m} - \theta_{i,j}^{n}}{\Delta t}\right\}, \tag{17}$$

$$(I + A_z)\psi^{n+1,2m+2} = \psi_{i,j}^{n+1,2m+1} + A_z\psi^{n+1,2m}, \tag{18}$$

where

$$\begin{aligned}
A_x\psi^{n+1,2m+1} &= -a_m\Delta_x(K^{n+1,2m}\Delta_x\psi^{n+1,2m+1}) \\
&= -\frac{a_m K_{i+1/2,j}^{n+1,2m}}{\Delta x^2}\left(\psi_{i+1,j}^{n+1,2m+1} - \psi_{i,j}^{n+1,2m+1}\right) \\
&\quad + \frac{a_m K_{i-1/2,j}^{n+1,2m}}{\Delta x^2}\left(\psi_{i,j}^{n+1,2m+1} - \psi_{i-1,j}^{n+1,2m+1}\right), \\
A_z\psi^{n+1,2m+2} &= -a_m\Delta_z(K^{n+1,2m}\Delta_z\psi^{n+1,2m+2}) \\
&= -\frac{a_m K_{i,j+1/2}^{n+1,2m}}{\Delta z^2}\left(\psi_{i,j+1}^{n+1,2m+2} - \psi_{i,j}^{n+1,2m+2}\right) \\
&\quad + \frac{a_m K_{i,j-1/2}^{n+1,2m}}{\Delta z^2}\left(\psi_{i,j}^{n+1,2m+2} - \psi_{i,j-1}^{n+1,2m+2}\right), \\
A_z\psi^{n+1,2m} &= -a_m\Delta_z(K^{n+1,2m}\Delta_z\psi^{n+1,2m}), \\
I\psi^{n+1,2m+2} &= \psi_{i,j}^{n+1,2m+2}.
\end{aligned} \tag{19}$$

The elimination of the predictor $\psi^{n+1,2m+1}$ from Eq. (17) by means of Eq. (18) gives

$$(I + A_x)(I + A_z)\psi^{n+1,2m+2} = \psi_{i,j}^{n+1,2m} + A_xA_z\psi^{n+1,2m} + a_m\left\{\Delta_z(K^{n+1,2m}) - \frac{\theta_{i,j}^{n+1,2m} - \theta_{i,j}^{n}}{\Delta t}\right\}. \tag{20}$$

Eq. (20) can be rewritten as the following one-pass form:

$$C_{i,j}^{n+1,2m}\frac{\psi_{i,j}^{n+1,2m+2}-\psi_{i,j}^{n+1,2m}}{\Delta t}+\frac{\theta_{i,j}^{n+1,2m}-\theta_{i,j}^{n}}{\Delta t}+I_m\overline{K}_{i,j}^{n+1,2m}\left(\psi_{i,j}^{n+1,2m+2}-\psi_{i,j}^{n+1,2m}\right)+a_mA_xA_z\left(\psi_{i,j}^{n+1,2m+2}-\psi_{i,j}^{n+1,2m}\right)=\Delta_x(K^{n+1,2m}\psi^{n+1,2m+2})+\Delta_z(K^{n+1,2m}\Delta_z\psi^{n+1,2m+2})+\Delta_z(K^{n+1,2m}). \quad (21)$$

Eq. (21) is equivalent to Eqs. (13) and (14), and this one-pass form is considerably similar to Eq. (5), which is linearized via the Picard iteration method. If the third and fourth terms of the left-hand side of Eq. (21) are neglected, Eqs. (21) and (5) become the same equation. The third and fourth terms are added upon the application of the IADI scheme and have a little significance when the iteratively updated value $\left(\psi_{i,j}^{n+1,2m+2}-\psi_{i,j}^{n+1,2m}\right)$ is sufficiently low. The AIADI scheme is a perturbation form of the Euler backward scheme linearized by the Picard method; it is expected that the behaviors of both these schemes are similar.

3. Numerical simulations

Five test simulations were performed for evaluating the performance of the proposed scheme. The performances of three different schemes were compared: the implicit scheme linearized by the Picard iteration method (Eq. (5)), the AIADI scheme (Eqs. (13) and (14)), and the original IADI scheme (Eqs. (9) and (10)).

The equation of Van Genuchten (1980) for the soil water retention curve and that of Mualem (1976) for the unsaturated hydraulic conductivity function were used in this study. The soil water retention curve is given by

$$S_e=\frac{\theta-\theta_r}{\theta_s-\theta_r}=\left\{\frac{1}{1+(\alpha|\psi|)^n}\right\}^{1-1/n}, \quad (22)$$

where S_e is the effective saturation; θ_r and θ_s are the residual and saturated water contents, respectively; and α and n are the Van Genuchten parameters, whose values depend upon the soil properties. Based on the model of Mualem (1976), the unsaturated hydraulic conductivity function is given by

$$K=K_sS_e^{1/2}\left\{1-\left(1-S_e^{n/(n-1)}\right)^{1-1/n}\right\}^2, \quad (23)$$

where K_s is the saturated hydraulic conductivity. The hydraulic conductivity of the boundary between the adjacent nodes is evaluated as

$$K_{i+1/2,j}=\frac{1}{2}(K_{i,j}+K_{i+1,j}). \quad (24)$$

The calculation of the hydraulic conductivity of the boundary could significantly affect the accuracy of the solution (Szymkiewicz, 2009). However, it is not supposed to affect the performance evaluation of the numerical schemes if the same method of calculation of the hydraulic conductivity is applied.

The time steps were adjusted automatically on the basis of the number of iterations required for convergence at the previous time step (Paniconi and Putti, 1994). The time step size cannot become less than a preselected minimum time step nor exceed a maximum time step. If the number of iterations to convergence is less than 4, the time step size for the next time step is increased by multiplying it with a predetermined value greater than 1 (1.2 in this study). If the number of iterations is greater than 7, the time step size for the next time step is multiplied by a preselected value less than 1 (0.83 in this study). If the number of iterations becomes greater than a prescribed maximum constant (20 in this study), the iterative process for the time level is terminated. Then, the time step size is reset to $\Delta t/3$, and the iterative process restarts.

A comparison of the relative accuracy of the numerical results obtained from different schemes is not easy (Lehmann and Ackerer, 1998). One of the most widely used criteria for evaluating the accuracy of a numerical scheme is the mass balance error (MBE) given by Celia et al. (1990):

$$\text{Mass Balance Error}=\left|1-\frac{\text{Total additional mass in the domain}}{\text{Total net flux into the domain}}\right| \quad (25)$$

where the total additional mass in the domain is the difference between the mass measured at any instant t and the initial mass in the domain, and the total net flux into the domain is the flux balance integrated in time up to t. Satisfying the mass balance is a necessary but not completely adequate prerequisite for a correct solution (Celia et al., 1990; Lehmann and Ackerer, 1998; Rathfelder and Abriola, 1994). Hence, the average relative error (ARE) and the maximum absolute error (MAE) are estimated as follows:

$$\text{Average relative error}=\frac{\sqrt{\sum_i(\bar{\psi}_i-\psi_i)^2}}{\sqrt{\sum_i\bar{\psi}_i^2}}, \quad (26)$$

$$\text{Maximum absolute error}=\max_i|\bar{\psi}_i-\psi_i|, \quad (27)$$

where ψ_i is the ith node solution obtained by using the models, and $\bar{\psi}_i$ is the ith node exact solution for the pressure head. In this paper, the analytical solution or the solution of dense grid was considered the exact solution. To use the solution of the dense grid as a surrogate for the exact solution, we confirmed that the solution of the relatively high-resolution grid as compared to the dense grid was very similar to that of the dense grid. The residual norm was estimated as follows:

$$\text{Residual norm}=\sum_i\Delta x\Delta z\left|(\theta_i^{n+1}-\theta_i^n)/\Delta t-\Delta_x(K^{n+1}\Delta_x\psi^{n+1})-\Delta_z(K^{n+1}\Delta_z\psi^{n+1})-\Delta_z(K^{n+1})\right|, \quad (28)$$

here ψ^{n+1}, θ^{n+1}, and K^{n+1} are the values after the iterative calculation.

In the test simulations 1, 2, 4, and 5, we used the soil properties shown in Table 1 by referring to Carsel and Parrish (1988). These represent the average values for the selected soil water retention and hydraulic conductivity parameters for the major soil textural groups.

3.1. Test 1: one-dimensional infiltration into dry soil

The accuracy of the proposed scheme was assessed through a one-dimensional infiltration simulation. Although the one-dimensional infiltration problem was considered to compare the result obtained by the proposed scheme with the analytical solution, a two-dimensional 1-m square domain was considered in this simulation because the proposed scheme is an algorithm for solving two- and three-dimensional problems. The traveling wave solution of Zlotnik et al. (2007) was considered as a exact solution. The merit of utilizing Zlotnik et al. (2007) is that the commonly used soil water retention curves such as that of Van Genuchten or Brooks-Corey can be used. Here, we used Van Genuchten's soil water

Table 1
Soil properties of major soil textures referring to Carsel and Parrish (1988).

Texture	θ_s m^3/m^3	θ_r m^3/m^3	K_s m/s	α m^{-1}	n
Sand	0.43	0.045	8.250×10^{-5}	14.5	2.68
Loamy sand	0.41	0.057	4.053×10^{-5}	12.4	2.28
Sandy loam	0.41	0.065	1.228×10^{-5}	7.5	1.89
Sandy Clay Loam	0.39	0.1	3.639×10^{-6}	5.9	1.48
Loam	0.43	0.078	2.889×10^{-6}	3.6	1.56
Silt	0.46	0.034	6.944×10^{-7}	1.6	1.37

retention curve and the sand soil texture in Table 1 was considered. The initial pressure head was $\psi_0 = -2$ m and the bottom boundary was set as $\psi(z = 0) = -2$ m. The upper boundary for the traveling wave solution was $\psi(z = \infty) - 0.1$ m, which is at the outside of the domain. Actually, the pressure head at the surface ($z = 1$ m) boundary was varied from -2 m to -0.1 m. Details of the surface boundary and the analytical solution can be found in Zlotnik et al. (2007). The other boundaries represent no-flux boundary conditions. The simulation period was 12 h. Six levels of grids were used: 10×10, 10×20, 10×40, 10×80, 10×160, and 10×320 grids.

Fig. 1 shows the results of ψ at the end of the simulations, and Table 2 shows the errors of the AIADI and the implicit schemes. The results of the AIADI and the implicit schemes with high-resolution grids agreed well with the analytical solution. However, relatively high values of errors were found when low-resolution grids were used. Infiltration into dry soil is a challenging problem; further, it is difficult to represent the sharp infiltration front with low-resolution grids. The results obtained from the two schemes were very similar, and the two schemes produced almost the same values of ARE and MAE. It was confirmed that the behaviors of the two schemes were similar as expected.

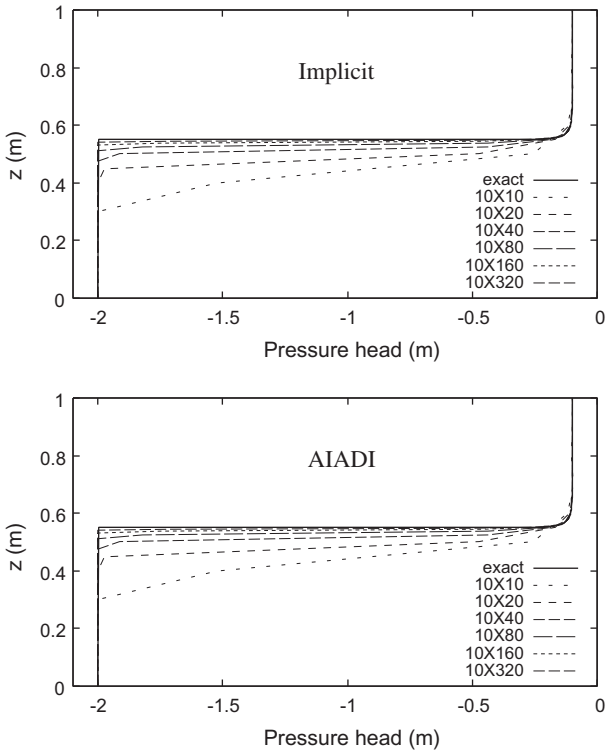

Fig. 1. Test simulation 1, ψ at the end of simulation.

Table 2
Test simulation 1, errors of the schemes.

Grid	Scheme	ARE[a] (%)	MAE[a] (m)
10×10	Implicit	36.85	1.74
	AIADI	36.85	1.74
10×20	Implicit	23.48	1.53
	AIADI	23.48	1.53
10×40	Implicit	16.99	1.56
	AIADI	16.99	1.56
10×80	Implicit	12.04	1.56
	AIADI	12.05	1.56
10×160	Implicit	8.40	1.53
	AIADI	8.40	1.53
10×320	Implicit	5.77	1.49
	AIADI	5.77	1.49

[a] ARE and MAE are evaluated at the end of simulation.

3.2. Test 2: infiltration into dry soil using the two-dimensional domain

The stability and the performance for different soil properties were assessed by simulating a two-dimensional infiltration problem. In this test, the 1-m square soil domain was considered, and the left-side surface ($0 < x \leqslant 25$ cm) was under a constant infiltration ($=K_s/2$) condition. The other boundaries represent no-flux boundary conditions. The initial pressure head used was $\psi(x,z,0) = -10.0$ m; four types of soil texture (sand, sandy loam, loam, silt) were used; and $\Delta x = \Delta z = 2.5$ cm. The simulation periods were 8 h (sand), 50 h (sandy loam), 100 h (loam), and 400 h (silt). To confirm the result, a simulation using the implicit scheme with a dense grid ($\Delta x = \Delta z = 0.5$ cm) was also performed.

Fig. 2 shows the result of ψ at the end of the simulation. A saturated–unsaturated flow was observed for sand and sandy loam, whereas only unsaturated flow was observed in the cases of loam and silt. The result calculated by each of the three schemes shows good agreement with the result of the implicit scheme obtained using the dense grid, although the IADI scheme incurs divergence in the cases of sand and sandy loam.

Fig. 3 describes the calculation time step. The AIADI and the implicit schemes had a similar time step. Oscillation was observed in the time step of the IADI scheme during the tests using sand and sandy loam. This oscillation occurred at 5 h 10 min for sand and at 37 h for sandy loam. Fig. 4 describes the water table position in both the cases. It is noted that the time when the oscillation began corresponds to the time when all bottom grids ($z = 0$) became saturated. It is implied that the IADI scheme might incur numerical instability when a saturated flow is simulated.

Table 3 shows the performances of each of the schemes. The AIADI scheme was faster than the implicit scheme in all four cases. All three schemes gave the same order of ARE and MAE. In the case of sand and sandy loam, the values of ARE and MAE were comparatively high, which can be attributed to the fact that a sharp infiltration front results in a high local error with relatively low-resolution grids. The IADI scheme exhibits a poor mass balance conservativity as compared to the other two schemes because the pressure-head-based Richards' equation is used. The MBE of the AIADI scheme was several orders higher than that of the implicit scheme in the cases of the saturated–unsaturated flow, sand, and sandy loam, while the other two schemes are based on the same mixed form of the Richards' equation. To investigate the reason for the above, the residual norm at each calculation time step was evaluated, which is shown in Fig. 5. In the case of the unsaturated flow, the implicit scheme and the AIADI scheme converged within the same order of the residual norm. However the AIADI scheme converged at a several orders higher level of the residual norm than the implicit scheme for the saturated–unsaturated flow. The appearances of the differences in the residual norm are simultaneous with the appearances of the saturated flow. Because the AIADI scheme is equivalent to Eq. (21), the different behavior between the AIADI and the implicit schemes should be attributed to the added terms for applying the ADI technique to the Richards' equation. The residual error caused by the added terms was evaluated from Eq. (21) as follows:

$$\text{Residual norm caused by added terms} = \sum_i \Delta x \Delta z \left| \left(I_m \overline{K}_i^{n+1,2m} + a_m A_x A_z \right) \left(\psi_i^{n+1,2m+2} - \psi_i^{n+1,2m} \right) \right|, \qquad (29)$$

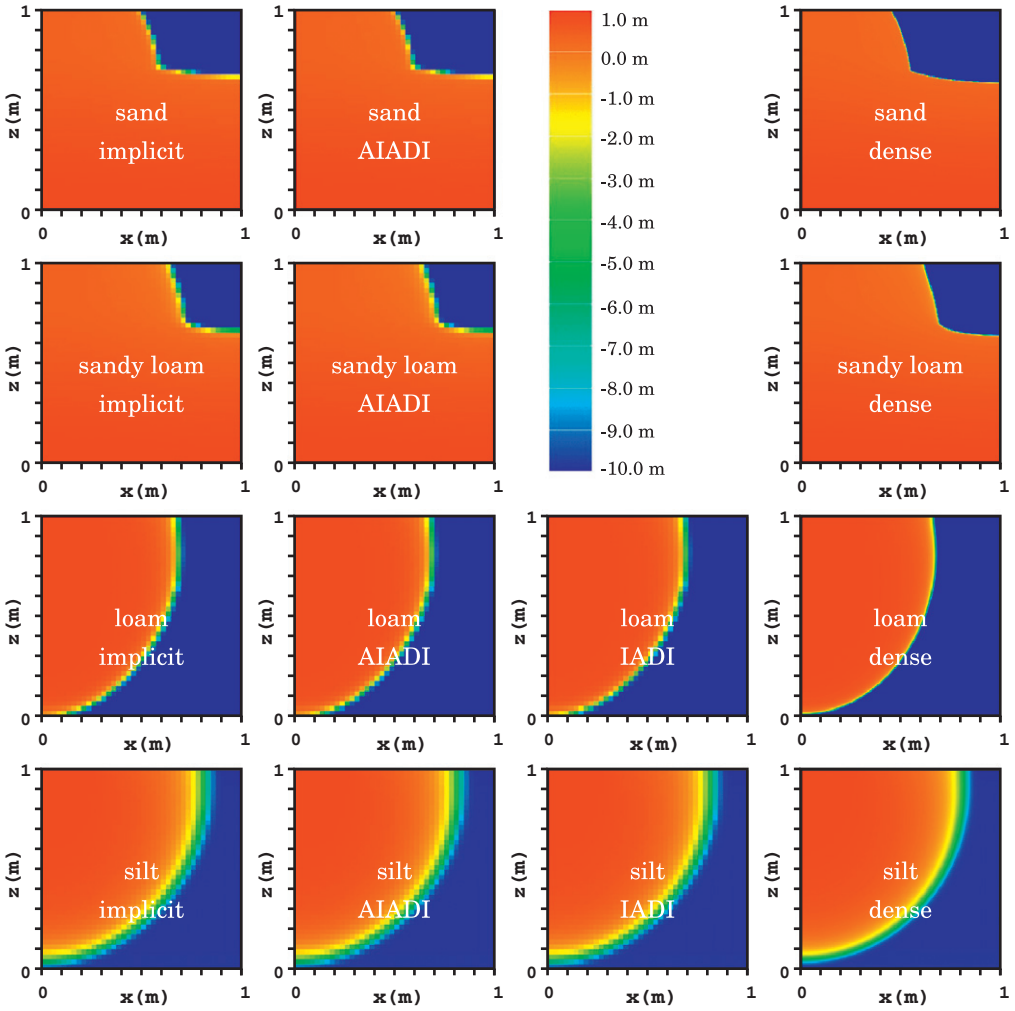

Fig. 2. Test simulation 2, ψ at the end of simulation.

where the iterative calculation converges at the iterative level $(2m + 2)$. Fig. 6 shows the total residual norm and the residual norm caused by the added terms. The added terms did not significantly contribute to the total residual norm in an unsaturated zone, but in a saturated zone it caused a comparatively larger residual norm, which resulted in a relatively large MBE. In the saturated zone, the value of K is larger than that in the unsaturated zone, which resulted in a relatively large $\overline{K}$, and the value of C became zero, which resulted in a relatively large a_m. Therefore, the effect of the added terms increases considerably in a saturated zone.

3.3. Test 3: transient variably saturated flow in two-dimensional domain

To investigate the performance for a saturated flow, the experiment conducted by Vauclin et al. (1979) was selected for the second test simulation. The same example was also used by Clement et al. (1994) to verify their two-dimensional variably saturated model. The model of Clement et al. (1994) and the implicit scheme considered in this paper represent the same algorithm. The flow domain consisted of a rectangular soil domain, 6.0 m × 2.0 m, with an initial horizontal water table located at a height of 0.65 m. At the soil surface, a constant flux of 148 mm/h was applied over a width of 1.0 m in the center. The remaining soil surface was covered to prevent the evaporation losses. Because of the symmetry, it was only necessary to model the right-hand side of the flow domain, as shown in Fig. 7. The modeled portion of the flow domain is 3.0 m × 2.0 m, with no flux on the bottom and the left-side boundaries.

The soil properties from Vauclin et al. (1979) are as follows: $\theta_s = 0.3$, $\theta_r = 0.01$, and $K_s = 9.72 \times 10^{-5}$ m/s. The van Genuchten model was fitted to the water retention and the relative hydraulic conductivity data given by Vauclin et al. (1979). The soil properties, $\alpha = 3.3\ \mathrm{m}^{-1}$, $n = 4.1$, estimated by Clement et al. (1994), were used along with $\Delta x = 10$ cm, $\Delta z = 5$ cm. The grid size of a dense grid was $\Delta x = 2$ cm, $\Delta z = 1$ cm. The simulation period was 8 h.

Fig. 7 describes the water table observed experimentally and calculated by each scheme at 0, 2, 3, 4, and 8 h. The results simulated using each of the three schemes closely agree with the experimentally observed values by Vauclin et al. (1979) and were themselves very similar to one another. Fig. 8 describes the calculation time step. A small oscillation in the time step was observed in the IADI scheme at around 3 h.

Table 4 shows the performance of the schemes. The AIADI was faster than the implicit scheme while it used a smaller time step and required more iteration steps. The AIADI generated a several orders higher MBE than the implicit scheme even though the obtained MBE is of a lower order than that of the IADI. This is coincident with the result of Test 2, in which the AIADI scheme leads to a comparatively larger MBE than the implicit scheme for a saturated flow in the cases of sand and sandy loam.

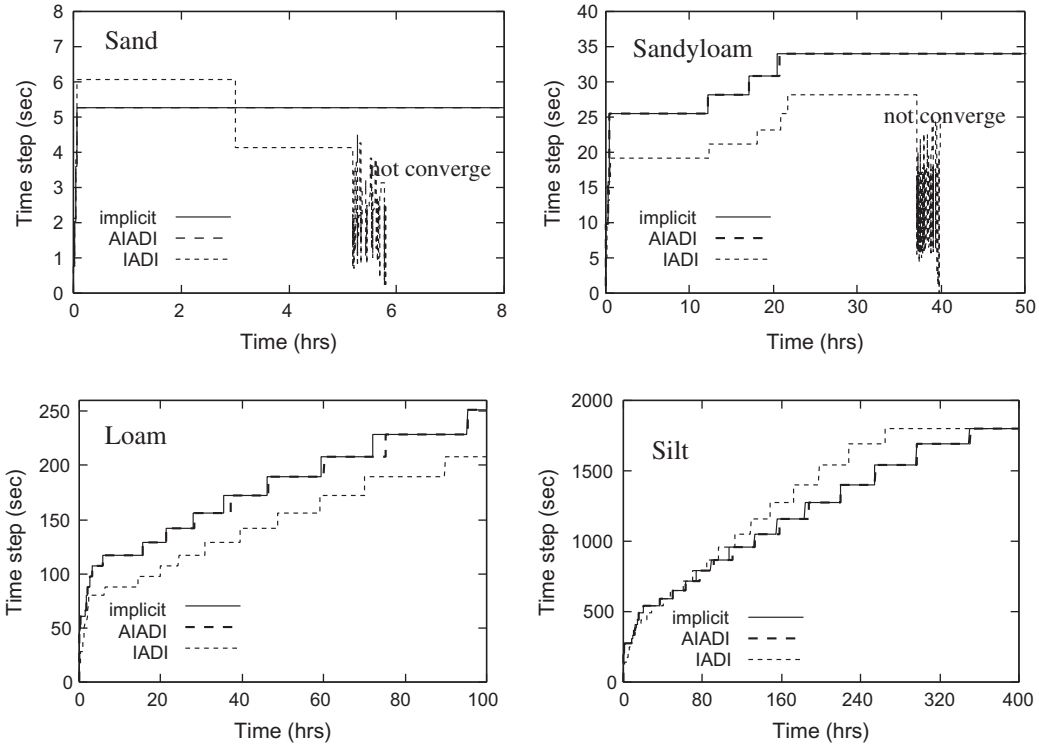

Fig. 3. Test simulation 2, time step.

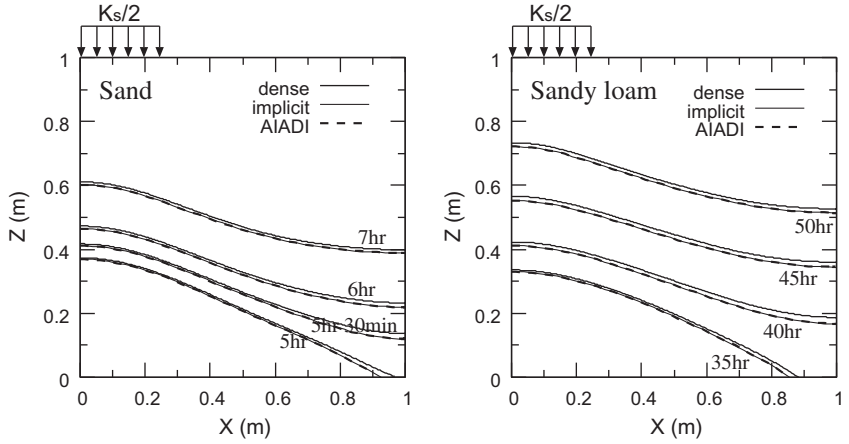

Fig. 4. Test simulation 2, water table positions in cases of sand and sandy loam.

Table 3
Test simulation 2, performances of the schemes.

Soil type (period)[a]	Scheme	CPU (s)	Nb.Iter[b]	MBE[c] (%)	ARE[c] (%)	MAE[c] (m)
Sand (8 h)	Implicit	532	22894	1.85e−08	38.13	9.75
	AIADI	184	22948	2.17e−04	38.14	9.75
Sandy loam (50 h)	Implicit	508	24073	6.28e−09	31.87	9.23
	AIADI	178	24076	2.16e−04	31.89	9.23
Loam (100 h)	Implicit	115	8797	2.61e−08	12.21	6.93
	AIADI	52	8848	7.71e−08	12.21	6.93
	IADI	77	11218	0.68	10.68	6.45
Silt (400 h)	Implicit	87	5820	1.02e−08	3.60	1.82
	AIADI	43	5857	7.96e−07	3.60	1.82
	IADI	40	5606	0.61	2.64	1.27

[a] (Period) is the simulation period.
[b] Nb.Iter is the total number of iteration.
[c] MBE, ARE, and MAE are evaluated at the end of simulation.

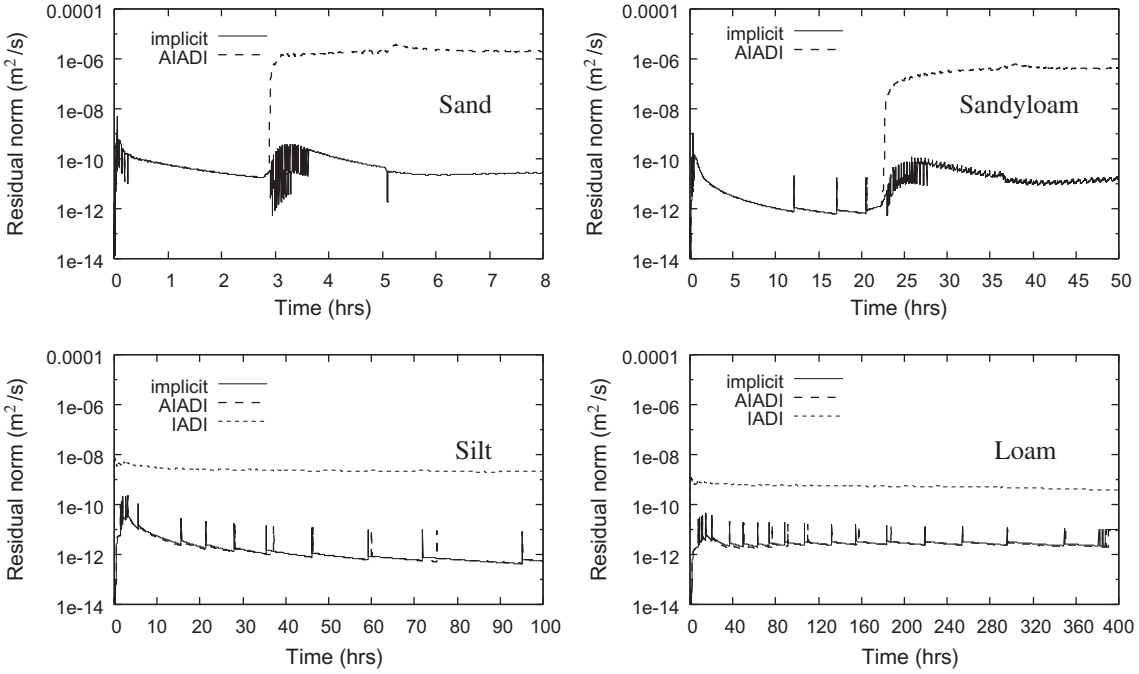

Fig. 5. Test simulation 2, residual norm at each calculation time step.

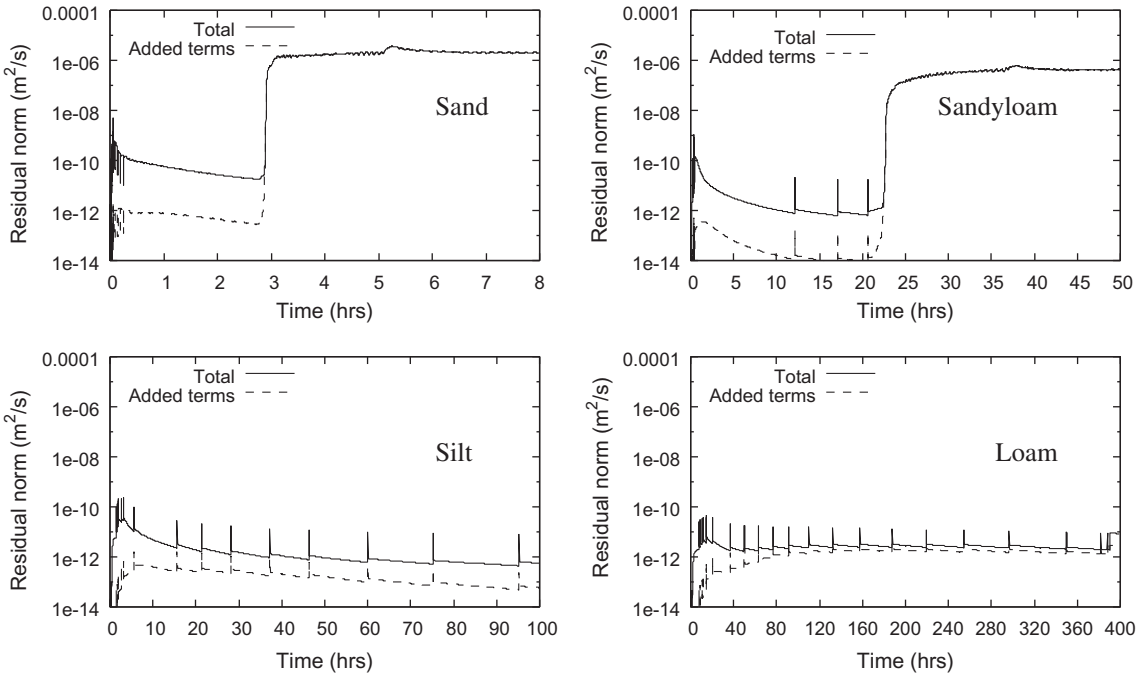

Fig. 6. Test simulation 2, total residual norm and residual norm caused by the added terms of AIADI scheme at each calculation time step.

3.4. Test 4: two-dimensional simulation for rainfall–infiltration on a simple slope

The simultaneous linear system solvers have a computational complexity of CN^a, where C and a are unknown constants and N is the number of unknowns in the linear system. The constant a of the AIADI scheme is expected to be very close to 1. To estimate the values of a of the two schemes, the implicit and AIADI schemes, a series of grid refinement experiments was conducted. The two-dimensional rainfall–infiltration simulation for a simple slope is considered. A 1-m-thick, 20-m-long slope with a 20-degree incline and a sandy loam soil texture was considered, as shown in Fig. 9a. A constant water level (30 cm) was maintained at the lower end for the sake of simplicity. The lower and upper sides were considered to be no-flux boundaries. The surface was given a rainfall–flux boundary condition, and the rainfall intensity is as shown in Fig. 9b. For an inclined slope, we used the modified coordinates, as shown in Fig. 9a, and the equation was given as

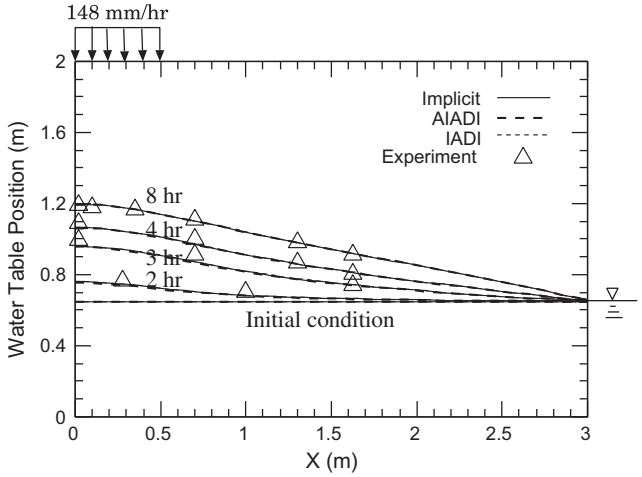

Fig. 7. Water-table mounding data collected by Vauclin et al. (1979) and simulated.

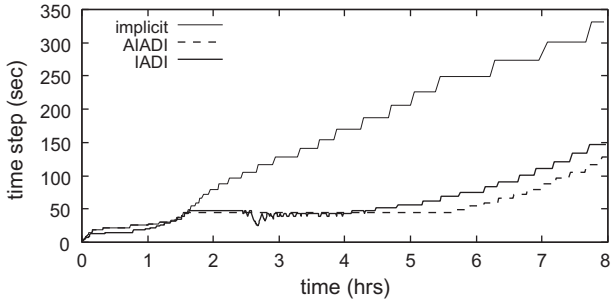

Fig. 8. Test simulation 3, time step.

$$\frac{\partial\theta}{\partial t} = \nabla\cdot K(\psi)\nabla\psi + \sin w\frac{\partial K(\psi)}{\partial x} + \cos w\frac{\partial K(\psi)}{\partial z}, \tag{30}$$

where w is 20 °. The initial condition was as follows: $\psi(x,z,0) + x\sin w + z\cos w = 30$ cm. The simulation period was two weeks. Six levels of grids were used: 100 × 20, 100 × 40, 200 × 40, 200 × 80, 400 × 80, and 400 × 160 grids. The 800 × 320 grid was used as the dense grid.

Fig. 10 describes the subsurface discharge from the lower end of the slope. It is confirmed that the AIADI and implicit schemes lead to a similar result. Table 5 shows the performances of the schemes. The AIADI scheme was faster than the implicit scheme and led to a several orders higher MBE than the implicit scheme such as in tests 1 and 2 while generating the same order of ARE and MAE. Fig. 11 shows the normalized CPU time divided by the number of cells

Table 4
Test simulation 3, performances of the schemes.

Scheme	CPU (s)	Nb.Iter[a]	MBE[b](%)	AREb (%)	MAE[b] (m)
Implicit	21	1520	2.24e−05	14.83	0.52
AIADI	10	3043	5.23e−02	14.80	0.52
IADI	12	3246	0.53	14.82	0.52

[a] Nb.Iter is the total number of iteration.
[b] MBE, ARE, and MAE are evaluated at the end of simulation.

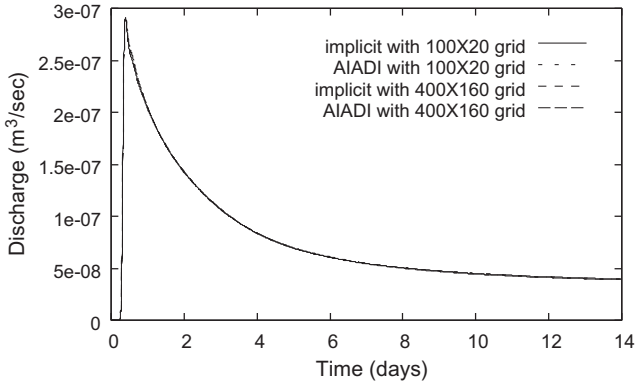

Fig. 10. Test simulation 4, discharge at the end of the slope.

and the total number of iterations. The value of a of the AIADI scheme was 1.04 and that of the implicit scheme was 1.36, which is compatible with our expectation. Therefore, as the number of unknowns increases, there is an increase in the relative efficiency of the AIADI scheme.

3.5. Test 5: three-dimensional infiltration into layered soil

The ability of simulating three-dimensional problems and flow for layered soil properties were tested. The 1-m cubic soil domain was considered, as shown in Fig. 12. The continuity of the flux and the pressure head were satisfied across the interface between two soils. The surface was taken to be under a constant infiltration (=5 mm/h) condition, and the other boundaries were under no-flux boundary conditions. The initial pressure head was taken as $\psi(x,y,z,0) = -2.0$ m. The time step was $1 \leqslant \Delta t \leqslant 3600$ s, and the simulation period was one day. Grid refinement was also applied in this test, where only the z direction refinement was conducted because this test is similar to the one-dimensional infiltration problem of the z-direction. Six levels of grids were used: 20, 40, 80, 160, 320, and 640 grids of the z-dimension; the x and

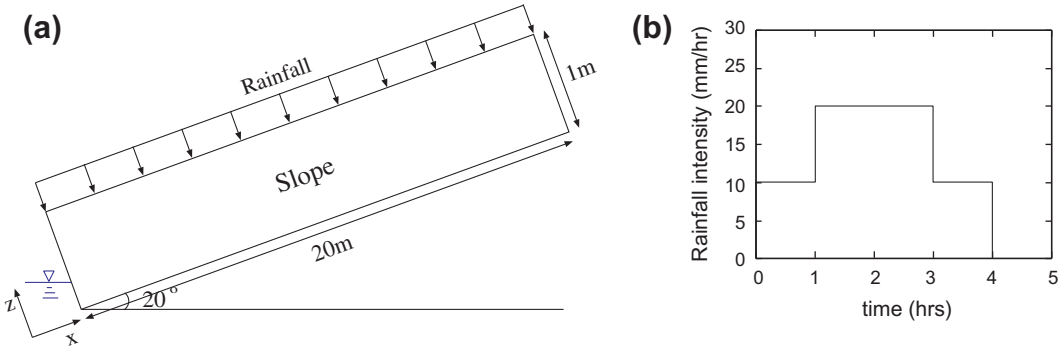

Fig. 9. Test simulation 4: (a) slope, (b) rainfall intensity.

Table 5
Test simulation 4, performances of the schemes.

Grid	Scheme	CPU (s)	Nb.Iter[a]	MBE[b] (%)	ARE[b] (%)	MAE[b] (m)
100 × 20	Implicit	23	3789	2.23e−08	46.62	5.61
	AIADI	18	3832	8.63e−05	47.09	5.61
100 × 40	Implicit	98	7071	1.58e−08	39.42	5.94
	AIADI	71	7071	3.68e−05	39.42	5.95
200 × 40	Implicit	303	7739	1.37e−08	30.67	5.58
	AIADI	162	7741	1.87e−05	30.67	5.58
200 × 80	Implicit	1716	14985	4.01e−09	25.95	5.74
	AIADI	572	15069	5.90e−05	25.26	5.71
400 × 80	Implicit	3761	15979	3.83e−09	16.64	4.93
	AIADI	1252	16051	2.87e−04	15.67	4.87
400 × 160	Implicit	21949	31900	5.99e−06	12.06	4.80
	AIADI	5579	31935	1.10e−04	12.05	4.80

[a] Nb.Iter is the total number of iteration.
[b] MBE, ARE, and MAE are evaluated at the end of simulation.

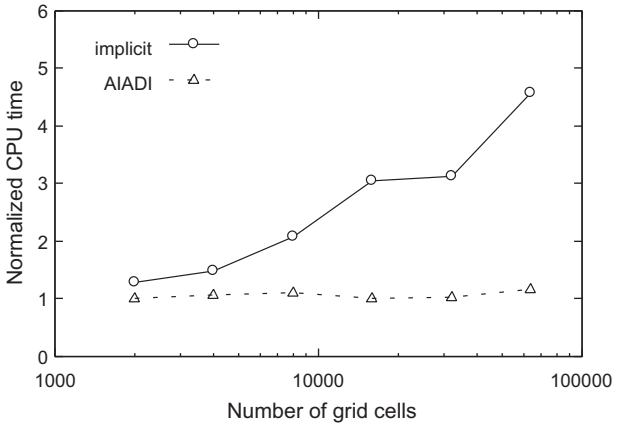

Fig. 11. Test simulation 4, normalized CPU time per iteration.

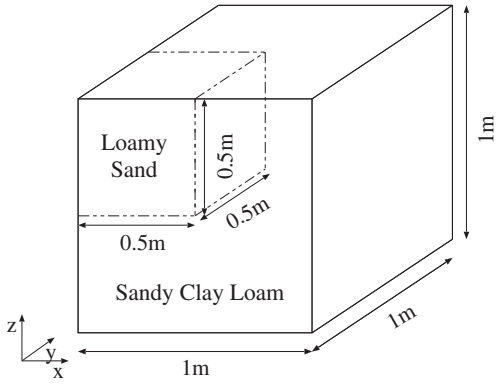

Fig. 12. Layered soil domain for test simulation 5.

y-dimension for all grids was 20 × 20. A 160 × 160 × 640 grid was used as the dense grid.

The three-dimensional AIADI equation consists of the following three passes:

$$C^{n+1,3m}_{i,j,k}\frac{\psi^{n+1,3m+1}_{i,j,k}-\psi^{n+1,3m}_{i,j,k}}{\Delta t}+\frac{\theta^{n+1,3m}_{i,j,k}-\theta^{n}_{i,j,k}}{\Delta t}+I_m\overline{K}^{n+1,3m}_{i,j,k}\left(\psi^{n+1,3m+1}_{i,j,k}-\psi^{n+1,3m}_{i,j,k}\right)=\Delta_x\left(K^{n+1,3m}\Delta_x\psi^{n+1,3m+1}\right)+\Delta_y(K^{n+1,3m}\Delta_y\psi^{n+1,3m})+\Delta_z(K^{n+1,3m}\Delta_z\psi^{n+1,3m})+\Delta_z(K^{n+1,3m}), \quad (31)$$

$$C^{n+1,3m}_{i,j,k}\frac{\psi^{n+1,3m+2}_{i,j,k}-\psi^{n+1,3m+1}_{i,j,k}}{\Delta t}+I_m\overline{K}^{n+1,3m}_{i,j,k}\left(\psi^{n+1,3m+2}_{i,j,k}-\psi^{n+1,3m+1}_{i,j,k}\right)=\Delta_y(K^{n+1,3m}\Delta_y\psi^{n+1,3m+2})-\Delta_y(K^{n+1,3m}\Delta_y\psi^{n+1,3m}), \quad (32)$$

$$C^{n+1,3m}_{i,j,k}\frac{\psi^{n+1,3m+3}_{i,j,k}-\psi^{n+1,3m+2}_{i,j,k}}{\Delta t}+I_m\overline{K}^{n+1,3m}_{i,j,k}\left(\psi^{n+1,3m+3}_{i,j,k}-\psi^{n+1,3m+2}_{i,j,k}\right)=\Delta_z(K^{n+1,3m}\Delta_z\psi^{n+1,3m+3})-\Delta_z(K^{n+1,3m}\Delta_z\psi^{n+1,3m}), \quad (33)$$

$$\overline{K}^{n+1,3m}_{i,j,k}=K^{n+1,3m}_{i+1/2,j,k}+K^{n+1,3m}_{i-1/2,j,k}+K^{n+1,3m}_{i,j+1/2,k}+K^{n+1,3m}_{i,j-1/2,k}+K^{n+1,3m}_{i,j,k+1/2}+K^{n+1,3m}_{i,j,k-1/2}, \quad (34)$$

where subscripts i, j, and k denote the spatial coordinates of the point in the x, y, and z axes, respectively. The three-dimensional implicit scheme linearized by the Picard method is given as

$$C^{n+1,m}_{i,j,k}\frac{\psi^{n+1,m+1}_{i,j,k}-\psi^{n+1,m}_{i,j,k}}{\Delta t}+\frac{\theta^{n+1,m}_{i,j,k}-\theta^{n}_{i,j,k}}{\Delta t}=\Delta_x(K^{n+1,m}\Delta_x\psi^{n+1,m+1})+\Delta_y(K^{n+1,m}\Delta_y\psi^{n+1,m+1})+\Delta_z(K^{n+1,m}\Delta_z\psi^{n+1,m+1})+\Delta_z(K^{n+1,m}). \quad (35)$$

In our experience, the traditional IADI scheme does not successfully converge for three-dimensional problems, e.g., a simple infiltration problem or rainfall–runoff problem even with a very low infiltration intensity and a small time step.

Fig. 13 describes the ψ calculated with the AIADI scheme with a 20 × 20 × 160 grid. A saturated zone did not appear in this test. Table 6 shows the performances of the schemes. The AIADI scheme performed faster than the implicit scheme in this three-dimensional test case. Fig. 14 shows the normalized CPU time. The value of a, defined in Section 3.4, of the AIADI scheme was almost 1 and that of the implicit scheme was 1.24 in this test. Furthermore, unlike in the case of a saturated flow such as Test 2–4, in the case of an unsaturated flow, the AIADI scheme generated the same order of MBE. For confirming that both schemes have the same accuracy in the case of an unsaturated flow, we evaluated the residual norm; it is shown in Fig. 15. Both schemes converged within the same order of residual norm at each calculation time step.

4. Conclusion

The performance of a new IADI algorithm for two- and three-dimensional saturated–unsaturated flows was evaluated. The proposed scheme based on the Douglas–Rachford ADI method is a perturbation form of the backward Euler difference equation linearized by the Picard method. The proposed scheme is

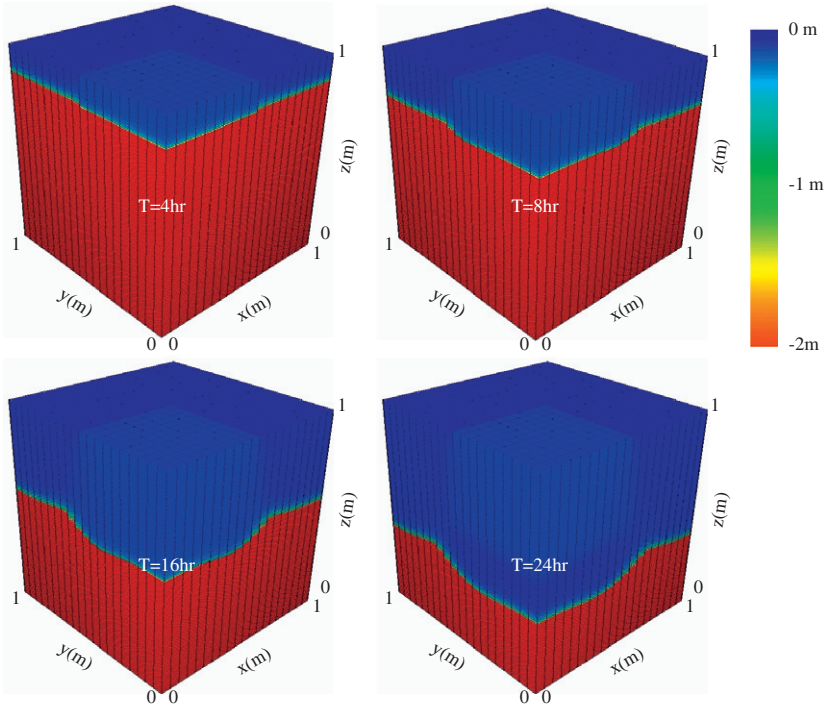

Fig. 13. Test simulation 5, ψ of vertical cross section for $y = 0$ calculated by the AIADI scheme with $20 \times 20 \times 160$ grid, where the inside of dashed line is loamy sand soil.

Table 6
Test simulation 5, performances of the schemes.

Grid (20×20)	Scheme	CPU (s)	Nb.Iter[a]	MBE[b] (%)	ARE[b] (%)	MAE[b] (m)
$\times 20$	Implicit	45	1719	6.64e−09	19.14	1.57
	AIADI	33	1718	1.67e−08	19.14	1.57
$\times 40$	Implicit	161	2830	3.92e−09	11.20	1.39
	AIADI	101	2830	1.35e−08	11.20	1.39
$\times 80$	Implicit	703	4959	2.50e−09	6.40	1.07
	AIADI	389	4959	6.15e−09	6.40	1.07
$\times 160$	Implicit	3125	9538	1.06e−09	3.28	0.89
	AIADI	1498	9538	1.60e−09	3.28	0.89
$\times 320$	Implicit	13990	18027	4.60e−10	2.86	0.90
	AIADI	5579	18158	5.49e−10	2.86	0.90
$\times 640$	Implicit	75419	38999	2.01e−10	2.58	0.89
	AIADI	21366	35137	1.94e−10	2.58	0.89

[a] Nb.Iter is the total number of iteration.
[b] MBE and RE are evaluated at the end of simulation.

mathematically clear and has certain advantages over the original IADI scheme in terms of applicability to three-dimensional problems. In order to eliminate the mass balance problem, the mixed form of the Richards equation was used. Because only tridiagonal linear systems are involved, the proposed scheme is simpler to implement and consumes less computational cost per iteration than the preconditioned Krylov solver. Additionally, the computational cost of the proposed scheme is expected to increase linearly when the problem dimension increases. Furthermore, parallelization for the proposed scheme is also very simple using a parallelization framework such as OpenMP. In the computation of a direction pass, each set of simultaneous equations can be calculated separately.

The performance of the proposed scheme was evaluated by conducting five test simulations. In some test cases, the original IADI scheme incurred numerical instability or divergence, but the proposed scheme exhibited stable behavior under the same

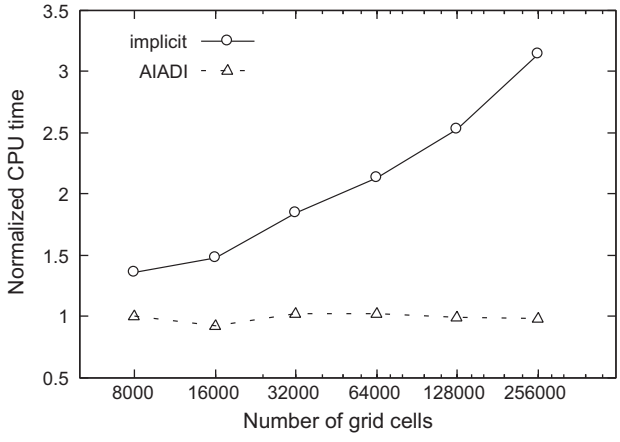

Fig. 14. Test simulation 5, normalized CPU time per iteration.

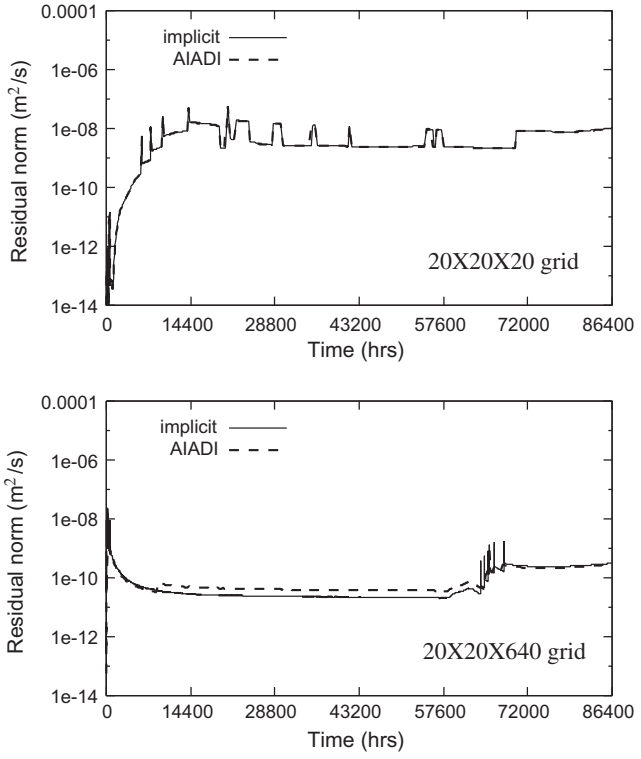

Fig. 15. Test simulation 5, residual norm at each calculation time step.

conditions. The proposed scheme can simulate a three-dimensional flow, whereas the original IADI scheme can only simulate a two-dimensional flow. This may be because the proposed scheme is derived from the Douglas–Rachford ADI scheme, which is unconditionally stable for two- and three-dimensional parabolic partial differential equations while the Peaceman–Rachford ADI scheme on which the original IADI scheme is based on is unconditionally stable only for two-dimensional equations. Although the stability is not guaranteed for the Richards' equation, it is empirically found that the proposed scheme is more stable than the original IADI scheme and is applicable to two- and three-dimensional saturated–unsaturated simulations.

The proposed scheme performed faster than did the Euler backward implicit scheme linearized by the Picard iteration method for all cases in which the linear systems were solved by an SSOR preconditioned BICGSTAB solver. As expected, the computational cost of the proposed scheme was proportional to the number of unknowns shown in Tests 3 and 4. However, in the saturated zone, the proposed scheme showed a comparatively lower numerical accuracy than the implicit scheme even though the proposed scheme converged within the same order of residual norm as that of the implicit scheme for unsaturated flows and gave the same order of MBE as shown in Tests 1 and 4. The added terms of the proposed scheme may cause the comparatively larger residual norm in the case of the saturated flow. There is a trade-off between the implicit scheme conserving the accuracy of the residual norm and the AIADI scheme consuming relatively few CPU resources and the ease of implementation.

The proposed scheme was applied only to relatively simple geometries that can be described by orthogonal grids. To overcome this disadvantage, further research is in progress to extend the proposed equation using a coordinate transformation method. We expect that a geometrically complex flow domain could be expressed by the extended model, whereas there is still a limitation as compared to the unstructured grid in the case when a highly complex geometry needs to be represented.

Acknowledgments

This work was supported by the Grant-in-aid for JSPS fellows and KAKENHI (20246082), Grant-in-aid for Scientific Research (A) of JSPS.

References

Bergamaschi, L., Putti, M., 1999. Mixed finite elements and Newton-type linearizations for the solution for the unsaturated flow equation. International Journal for Numerical Methods in Engineering 45, 1025–1046.
Carsel, R.F., Parrish, R.S., 1988. Developing joint probability distributions of soil water retention characteristics. Water Resources Research 24, 755–769.
Celia, M.A., Bouloutas, E.T., Zarba, R.L., 1990. A general mass-conservative numerical solution for the unsaturated flow equation. Water Resources Research 26 (7), 1483–1496.
Clement, T.P., Wise, W.R., Molz, F.J., 1994. A physically based, two-dimensional, finite difference algorithm for modeling variably saturated flow. Journal of Hydrology 161, 69–91.
Cooley, R.L., 1971. A finite difference method for unsteady flow in variably saturated porous media: application to a single pumping well. Water Resources Research 7, 1607–1625.
Dane, J.H., Mathis, F.H., 1981. An adaptive finite difference scheme for the one-dimensional water flow equation. Soil Science Society of America 45, 1048–1054.
Dogan, A., Motz, L.H., 2005. Saturated–unsaturated 3D groundwater model. I: Dvelopment. Journal of Hydrologic Engineering 10 (6), 492–504.
Douglas, J., Rachford, H.H., 1956. On the numerical solution of heat conduction problems in two and three space variables. Transactions of the American Mathematical Society 82 (2), 421–439.
Fassino, C., Manzini, G., 1998. Fast-secant algorithms for the non-linear Richards equation. Communications in Numerical Methods in Engineering 14, 921–930.
Forsyth, P.A., Wu, Y.S., Pruess, K., 1995. Robust numerical methods for saturated-unsaturated flow with dry initial conditions in heterogeneous media. Advances in Water Resources 18, 25–38.
Haverkamp, R., Vauclin, M., 1981. A comparative study of three forms of the Richards equation used for predicting one-dimensional infiltration in unsaturated soil. Soil Science Society of America 45, 13–20.
Jie, Y., Jie, G., Mao, Z., Li, G., 2004. Seepage analysis based on boundary-fitted coordinate transformation method. Computers and Geotechnics 31, 279–283.
Jones, J.E., Woodward, C.S., 2001. Newton-Krylov-Multigrid solvers for large-scale, highly heterogeneous, variably saturated flow problems. Advances in Water Resources 24, 763–774.
Kavetski, D., Binning, P., Sloan, S.W., 2002. Noniterative time stepping schemes with adaptive truncation error control for the solution of Richards equation. Water Resources Research 24, 595–605.
Kinouchi, T., Kanda, M., Hino, M., 1991. Numerical simulation of infiltration and solute transport in an s-shaped model basin by a boundary-fitted grid system. Journal of Hydrology 122, 373–406.
Koo, M., Leap, D.I., 1998a. Modeling three-dimensional groundwater flows by the body-fitted coordinate (BCF) method: I. Stationary boundary problems. Transport in Porous Media 30, 217–239.
Koo, M., Leap, D.I., 1998b. Modeling three-dimensional groundwater flows by the body-fitted coordinate (BCF) method: II.free and moving boundary problems. Transport in Porous Media 30, 345–362.
Kotakemori, H., Hasegawa, H., Nishida, A., 2005. Performance evaluation of aparallel iterative method library using OpenMP. In Proceedings of the 8th International Conference on High Performance Computing in Asia Pacific Region. pp. 432–436.
Lehmann, F., Ackerer, P.H., 1998. Comparison of iterative methods for improved solutions of the fluid flow equation in partially saturated porous media. Transport in Porous Media 31, 275–292.
Li, M., Cheng, H., Yeh, G., 2000. Solving 3D subsurface flow and transport with adaptive multigrid. Journal of Hydrologic Engineering 5 (1), 74–81.
Manzini, G., Ferraris, S., 2004. Mass-conservative finite volume methods in 2-D unstructured grid for the Richards equation. Advances in Water Resources 27, 1199–1215.
Mualem, Y., 1976. A new model for predicting hydraulic conductivity of unsaturated porous media. Water Resources Research 12, 513–522.
Paniconi, C., Putti, M., 1994. A comparison of Picard and Newton iteration in the numerical solution of multidimensional variably saturated flow problems. Water Resources Research 30 (12), 3357–3374.
Parissopoulos, G.A., Wheater, H.S., 1988. On numerical errors associated with the iterative alternating direction implicit(IADI) finite difference solution of the two dimensional transient saturated-unsaturated flow(Richards) equation. Hydrological Processes 2, 187–201.
Peaceman, D.W., Rachford, H.H., 1955. The numerical solution of parabolic and elliptic differential equations. Journal of the Society for Industrial and Applied Mathematics 3 (1), 28–41.
Perrens, S.J., Watson, K.K., 1977. Numerical analysis of two-dimensional infiltration and redistribution. Water Resources Research. 13, 781–790.
Rathfelder, K., Abriola, L.M., 1994. Mass conservative numerical solutions of the head-based Richards equation. Water Resources Research 30 (9), 2579–2586.

Rubin, J., 1968. Theoretical analysis of two-dimensional transient flow of water in unsaturated and partly unsaturated soil. Soil Science Society of America 32, 610–615.

Ruhaak, W., Rath, V., Wolf, A., Clauser, C., 2008. 3D finite volume groundwater and heat transport modeling with non-orthogonal grids, using a coordinate transformation method. Advances in Water Resources 31, 513–524.

Richards, L.A., 1931. Capillary conduction of liquids of through porous medium. Physics 1, 318–333.

Simunek, J., Sejna, M., Van Genuchten, M.T., 1999. HYDRUS-2D: simulating water flow and solute transport in two-dimensional variably saturated media. Tech, Res., IGWMC, Golden, CO, USA.

Szymkiewicz, A., 2009. Approximation of internodal conductivities in numerical simulation of one-dimensional infiltration, drainage, and capillary rise in unsaturated soils. Water Resources Research 45, W10403. doi:10.1029/2009WR0007654.

Tocci, M.D., Kelley, C.T., Miller, C.T., 1997. Accurate and economical solution of the pressure-head form of Richards' equation by the method of lines. Advances in Water Resources 20, 1–14.

Van Genuchten, M.T., 1980. A closed-form equation for predicting the hydraulic conductivity of unsaturated soils. Soil Science Society of America 44, 892–898.

Vauclin, M., Khanji, D., Vachaud, G., 1979. Experimental and numerical study of a transient, two-dimensional unsaturated-saturated water table recharge problem. Water Resources Research 15 (5), 1089–2001.

Weeks, S.W., Sander, G.C., Braddock, R.D., Matthews, C.J., 2004. Saturated and unsaturated water flow in inclined porous media. Environmental Modeling and Assessment 9, 91–102.

Zlotnik, V.A., Wang, T., Nieber, J.L., Simunek, J., 2007. Verification of numerical solutions of the Richards equation using a traveling wave solution. Advances in Water Resources 30, 1973–1980.